27 May 2010, 4:30 pm - 6:20 pm

Microscale Characterization of Energy Dissipation Mechanisms During Liquefaction

Usama El Shamy
Southern Methodist University, Dallas, TX

Christina Denissen
U.S. Nuclear Regulatory Commission: Region IV, Arlington, TX


Fifth International Conference on
Recent Advances in Geotechnical Earthquake Engineering and Soil Dynamics
and Symposium in Honor of Professor I.M. Idriss
May 24-29, 2010 • San Diego, California

MICROSCALE CHARACTERIZATION OF ENERGY DISSIPATION MECHANISMS DURING LIQUEFACTION

Usama El Shamy
Southern Methodist University
Dallas, TX 75275

Christina Denissen
U.S. Nuclear Regulatory Commission: Region IV
Arlington, TX 76011

ABSTRACT

This study utilizes the discrete element method (DEM) to present a microscopic energy monitoring approach to characterize energy dissipation mechanisms in seismically loaded soils. Numerical simulations were conducted on saturated deposits of granular particles subjected to seismic excitations, modeled using a transient fully-coupled continuum-fluid discrete-particle model. The onset of liquefaction is illustrated through macroscopic and microscopic response patterns. An in-depth look at the individual microscale energy components both before and after the onset of liquefaction is presented. Prior to liquefaction, energy is dissipated mainly through inter-particle sliding (friction energy), but after liquefaction particle-to-particle impact damping also plays a major role in dissipating energy.

INTRODUCTION

Since it's first application to granular systems by Cundall and Strack in 1979, the discrete element method (DEM) has been utilized by researchers in geotechnical engineering to model soil systems as an assembly of discrete particles. DEM models have been widely used in the analysis of dry cohesionless soils (Bathurst and Rothenburg, 1988; Dobry and Ng, 1992; Thornton and Liu, 2000) and have also been employed to investigate the undrained response of saturated granular soils (Ng, 1989; Evgin, 2000). Coupling of pore-fluid with DEM was presented to analyze fluid flow in saturated soils by El Shamy and Zeghal (2005a) as well as the dynamic response and liquefaction of saturated granular deposits (El Shamy and Zeghal, 2005b, 2007). These successful applications of DEM highlight its ability to accurately model granular soils and investigate complex response mechanisms.

The main strength of DEM-based simulations lies in their ability to provide a great deal of information at the microscale that can be retrieved at any time during the simulation. In this regard, energy monitoring could serve as a powerful tool to investigate the response of soil systems during an intricate phenomenon such as liquefaction. By means of monitoring energy components, a comprehensive assessment of the response of soils to dynamic loading can be attained. Additionally, energy monitoring enhances the understanding of the response of the system at multiple stages during the seismic loading and assures energy balance.

In geotechnical engineering, energy-based methods have emerged as an approach for assessing liquefaction potential. Nemat-Nasser and Shokooh (1979) were first to present a unified theory for densification and liquefaction of a homogeneous sample of cohesionless sand based on energy considerations. Researchers have since then attempted to examine the possible application of the energy concept in the evaluation of liquefaction potential (e.g., Davis and Berrill, 1982; Law and Cao, 1990; Figueroa, 1990). Figueroa and co-workers (Figueroa *et al*., 1994; Liang et al., 1995) performed torsional shear tests on sand specimens subjected to sinusoidal and random cyclic loadings and formulated generalized equations relating the energy per unit volume required for liquefaction to occur with specific parameters of the soil and the loading characteristics. Thevanayagam *et al*. (2003) presented one of the early attempts to characterize liquefaction potential based on a microscale analytical model. They calculated energy dissipation due to inter-grain frictional sliding for idealized granular samples composed of regular array arrangements. Their approach, however, was limited by the difficulty of relating random particle size distributions to results of regular arrays.

In order to accurately predict the response of soil systems, an understanding of the micromechanical behavior of the soil in the time leading up to liquefaction is needed. This study presents a microscale energy monitoring approach to characterize the several forms of energy dissipation

mechanisms in saturated granular soils subjected to dynamic excitation. The macroscopic and microscopic response patterns of the deposit to seismic loading are first presented. A detailed description of the evolution of microscale energy components both before and after liquefaction takes place is discussed, and an interpretation of the relationship between the components is provided.

METHODOLOGY

Saturated granular soils were idealized as two overlapping media. The solid phase was modeled as an assemblage of discontinuous particles using the discrete element method, DEM (Cundall and Strack, 1979). The pore fluid was considered to be inviscid and incompressible, and was idealized using averaged Navier-Stokes equations of conservation of mass and momentum (e.g., Jackson, 2000):

$$\frac{\partial n}{\partial t} + \frac{\partial (n u_i)}{\partial x_i} = 0 \qquad (1)$$

$$\frac{\partial (n u_i)}{\partial t} + \frac{\partial (n u_i u_j)}{\partial x_j} = -\frac{n}{\rho}\frac{\partial p}{\partial x_i} + n\rho g_i + d_i \qquad (2)$$

along with appropriate boundary and initial conditions. In Eqs. (1) and (2), x_i (i=1,2,3) are Cartesian coordinates, n is porosity, u_i is fluid velocity, ρ is fluid density, p is fluid pressure, and g_i is gravitational force per unit mass. The term d_i represents averaged fluid-particle interaction force per unit of volume and was accounted for by using well established semi-empirical relationships proposed by Ergun (1952) and Comiti and Renaud (1989).

An explicit time-integration scheme was used to evaluate the coupled fluid-particle response. The fluid domain was discretized into parallelepiped cells and averaged Navier-Stokes equations were solved using a finite volume technique. Average drag forces exerted by the fluid on the particles within a specific cell were evaluated based on mean values of porosity, as well as of particle sizes and velocities within this cell. These forces were then applied to each of the individual particles proportionally to their volumes. Deformation of the solid phase subjected to the drag forces along with any external loads was subsequently computed using the DEM technique (Itasca, 2005). Details of the implemented continuum-discrete model are given in (El Shamy and Denissen, 2009a).

ENERGY COMPONENTS

Energy monitoring enhances understanding of the interaction of particles at the microscale and provides means to understand response mechanisms at the macroscale. Additionally, monitoring the individual energy components assures energy conservation and quantifies the contribution of each energy term to the total dissipated energy. Despite an extensive number of research studies in the geotechnical field utilizing DEM, very little has been done in terms of energy monitoring. In other engineering fields, like powder technology, few studies have investigated energy (Zhang and Whiten, 1998; Rajamani *et al*., 2000; Yanadida *et al*., 2001), mostly looking at potential and kinetic energies of powder beds subjected to vibration. Asmar *et al*. (2003) provided perhaps the most complete energy monitoring study thus far, developing a detailed energy bookkeeping scheme and applying it to a DEM simulation of vibrating particles, tracking kinetic energy, gravitational potential energy, contact strain energy, dissipated energy due to damping and gross frictional sliding, and the work done by the boundary walls on the particle system. They were able to verify energy conservation and concluded that energy was dissipated mainly through normal damping and gross sliding during vibration of granular materials. El Shamy and Denissen (2009b) monitored microscale energies of granular soil samples in a cyclic triaxial test environment. Under undrained conditions and no gravity assumptions, only boundary, friction, and elastic strain energies were considered. They quantified the total microscopic energy dissipated from the synthetic soil samples as a means to evaluate granular soils for liquefaction potential. In this paper, this approach is extended to saturated soil systems. The energies considered in this study are body, boundary, friction, kinetic, normal strain, shear strain, impact damping, and fluid-drag energies (Table 1).

SIMULATIONS

A semi-infinite deposit was idealized by computationally pluviating particles within a parallelepiped domain having periodic boundaries in the two lateral directions (Fig. 1) to mimic its infinite lateral extent in the two lateral directions. The periodic deposit consists of relatively large spherical grains subjected to a high gravitational field in order to get the number of particles to a computationally manageable size. The employed high g-level mimics the conditions of centrifuge testing of small-scale geotechnical models. Specifically, a 190 mm high deposit of particles, having an average diameter of 6 mm and saturated with a viscous fluid, was subjected to a dynamic base excitation under a gravity field of 30g. The pore fluid has a viscosity of 4.98 Pa s to compensate for the effects of the employed 30g level and large particle size (El Shamy, 2004). The analyzed model corresponds to a semi-infinite periodic prototype of a 5.70 m granular deposit. The computational details of the conducted simulations are given in (El Shamy and Denissen, 2009a).

Table 1. Summary of energy components

Energy component	Description	Equation	Reference
Body energy, E_b	Energy resulting from body forces (gravity)	$E_b = \sum_{t-0}^{t} \sum_{p=1}^{N_p} m_p \mathbf{f}_g^T d\mathbf{u}_p$	Itasca (2005)
Boundary energy, E_w	Energy resulting from work done by boundaries (walls) on particles	$E_w = \sum_{t=0}^{t} \sum_{w=1}^{N_w} \mathbf{f}_w^T d\mathbf{u}_w + \mathbf{m}_w^T d\boldsymbol{\theta}_w$	Itasca (2005)
Frictional energy, E_f	Energy dissipated by frictional sliding at all particle-to-particle contacts	$E_f = \sum_{t-0}^{t} \sum_{c=1}^{N_c} \mathbf{f}_s^T d\mathbf{u}_{slip}$	Itasca (2005)
Kinetic energy, E_k	Total kinetic energy of all particles accounting for both translational and rotational motion	$E_k = \frac{1}{2} \sum_{p=1}^{N_p} m_p \dot{\mathbf{u}}_p^2 + I_p \dot{\theta}_p^2$	Itasca (2005)
Strain energy, E_s	Total strain energy of the entire assembly stored at all contacts	$E_s = \frac{1}{2} \sum_{c=1}^{N_c} \frac{\mathbf{f}_n^2}{k_n} + \frac{\mathbf{f}_s^2}{k_s}$	Itasca (2005)
Damping energy, E_d	Energy dissipated due to particle-to-particle impacts at all contacts	$E_d = \sum_{t=0}^{t} \sum_{c=1}^{N_c} \mathbf{e} d\mathbf{u}_n$	El Shamy and Denissen (2009a)
Fluid-drag energy, E_i	Energy due to fluid-particle interactions resulting from applied drag forces $\mathbf{f}_d$	$E_i = \sum_{t=0}^{t} \sum_{p=1}^{N_p} \mathbf{f}_d^T d\mathbf{u}_p$	El Shamy and Denissen (2009a)

N_p is number of particles, N_c is number of contacts, N_w is number of walls, $d\mathbf{u}_p$ is incremental particle displacement vector, $d\theta_p$ is incremental particle rotation vector, $d\mathbf{u}_w$ is incremental wall displacement vector, $d\theta_w$ is incremental wall rotation vector, $\mathbf{f}_s$ is contact shear force vector, $\mathbf{f}_s$ is contact normal force vector, k_n and k_s are contact normal and shear stiffness respectively, $\mathbf{e}$ is normal damping force vector at the contact, $d\mathbf{u}_n$ is incremental relative displacement vector at the contact, and $d\mathbf{u}_{slip}$ is incremental slip displacement vector at the sliding contact.

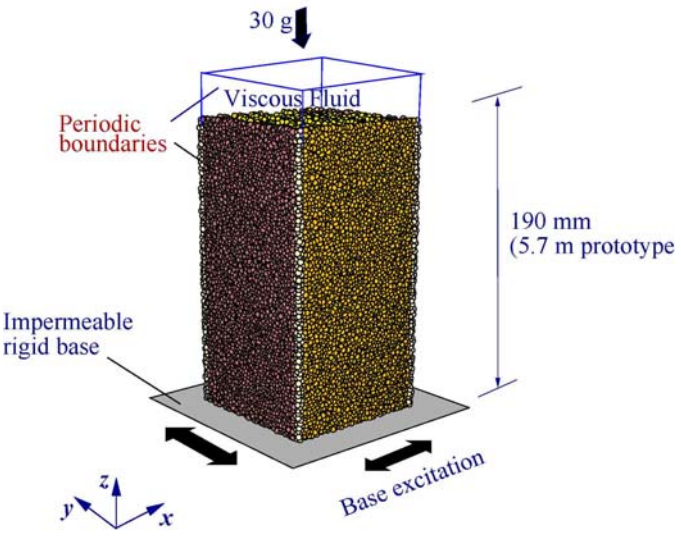

Fig. 1. Three-dimensional view of the particle deposit employed in the conducted simulation.

The deposit was subjected to a dynamic base excitation that resembles a periodic (sinusoidal) loading pattern. The excitation was applied in the two lateral directions (*x* and *y*) in order to mimic actual seismic loading conditions. The sinusoidal input signal gradually increases until reaching the maximum acceleration of 0.1g at 4.5 s, where it remains constant until the cyclic loading is stopped at 12 s. The input motion in the *y*-direction has exactly the same pattern as the *x*-direction but with a phase lag of 90°. Figure 2 shows the acceleration in the *y*-direction versus the acceleration in the *x*-direction for the sinusoidal loading signal. The spiral pattern is the result of the gradually increasing sinusoidal acceleration in each direction until the maximum amplitude of 0.1g is reached, after which the accelerations follow the outermost circular path until returning to zero at the end of shaking.

Seismic response

The input motion and computed time histories of averaged particle accelerations in both lateral directions are shown in Fig. 3 at selected depth locations. These time histories have been filtered to eliminate frequency components higher than 4

Hz. At all depths the accelerations vanish, indicating that the deposit liquefied and prevented the base excitation from propagating upward. The strata liquefied at slightly different time instants, however, liquefying first near the surface and last at the base. For instance, the accelerations of the stratum at a depth location of 0.9 m from the surface disappeared at 2.28 s while the accelerations at a depth of 4.8 m disappeared at 2.63 s. Note that all depth locations liquefied prior to the input signal reaching the maximum acceleration of 0.1g.

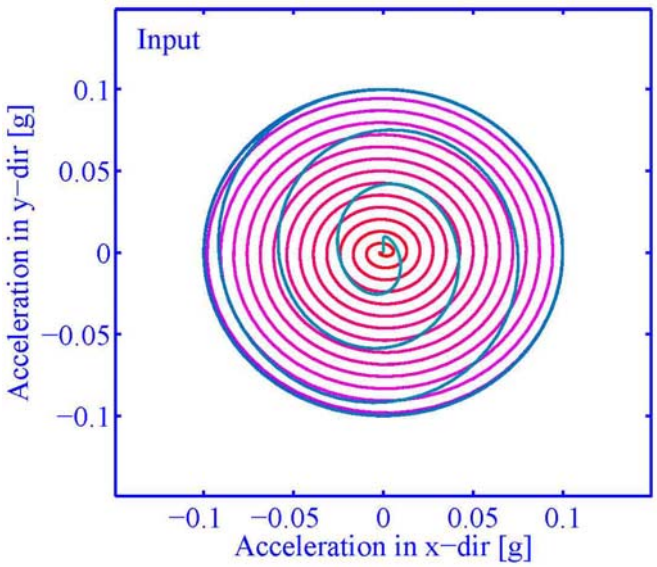

Fig. 2. Trajectory of input accelerations on the x-y plane.

The buildup of excess pore-water pressure, Du, is an important indicator to characterize the onset of liquefaction. Liquefaction is commonly defined as the instant at which the excess pore pressure ratio approaches a value of one, at which time the pore pressure has counterbalanced the effective stress and there are no inter-particle contact forces. Figure 4 shows the time histories of excess pore-water pressure ratio at a number of depth locations in the deposit (filtered at 4 Hz). The response indicates that a pore pressure ratio of one was reached for the entire deposit, indicating liquefaction at all depths. Again the onset of liquefaction occurred at slightly different time instances depending on depth, liquefying first at the surface, and last near the base. The time to liquefaction for all featured depths is in agreement with the acceleration time histories of Fig. 3. Liquefaction of the analyzed deposit was associated with a significant surface settlement that persisted after the shaking had ended. Total settlement was about 136 mm and was reached at about 30 s after the excitation stopped.

Cyclic shear stress trajectories from the stresses acting on the *xy* planes are shown in Fig. 5 for the same selected depth locations. The stress amplitude increases with depth, which is expected due to the increase in confining pressure. At a given depth location the stresses also increase with each cycle as the acceleration of the base wall gradually increases. As liquefaction takes place, the shear stresses vanish as contacts are lost between particles. The number of cycles prior to liquefaction is about 7 cycles at a depth location of 0.9 m and about 8 cycles at a depth location of 4.8 m. These results are consistent with time histories of particle acceleration and excess pore-water pressure ratio discussed above.

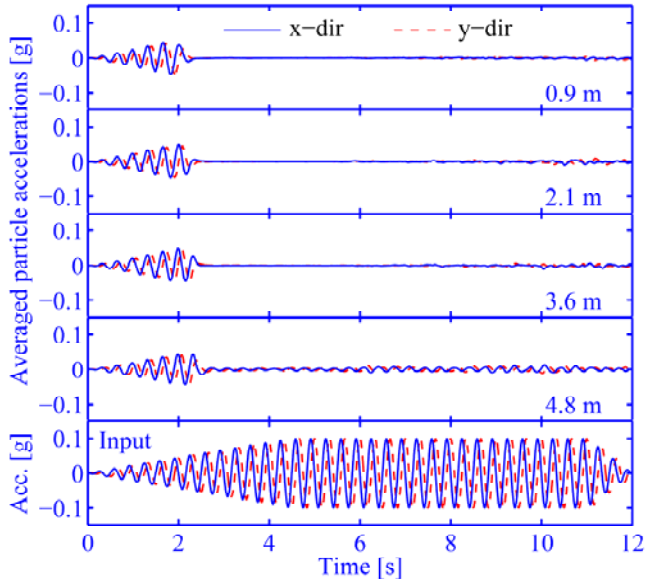

Fig. 3. Time histories of acceleration in the x and y-directions at selected depth locations.

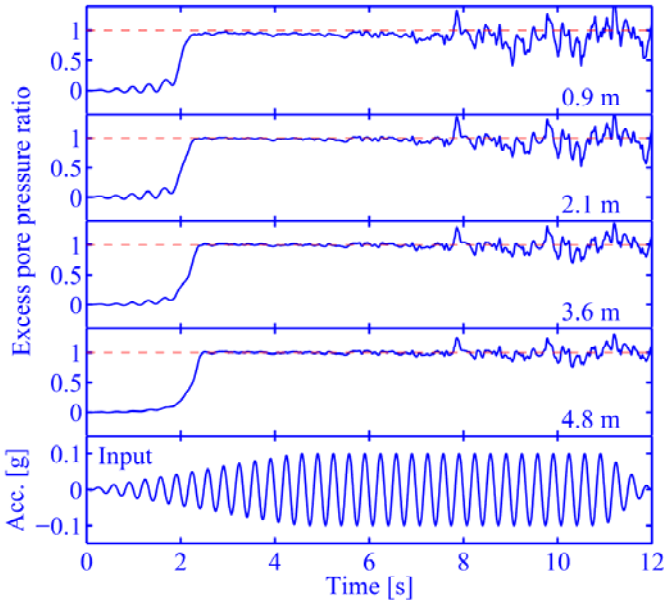

Fig. 4. Time histories of excess pore pressure ratio at selected depth locations.

From a microscale point of view, liquefaction at a specific location is associated with a decrease in the number of contacts between particles until the particles are essentially floating and a relatively small number of contacts occur between the particles. The time history of coordination number (average number of contacts per particle) is shown in Fig. 6. For frictional spherical particles, a coordination number of four is required to maintain a stable packing (Edwards, 1998). The figure shows that the deposit maintains a coordination number well above 4 for the first two seconds of shaking, after which the contacts, and therefore coordination number, quickly drop to unstable conditions, indicating that liquefaction has taken place. The coordination number time histories confirm that liquefaction is steadily delayed as the depth increases.

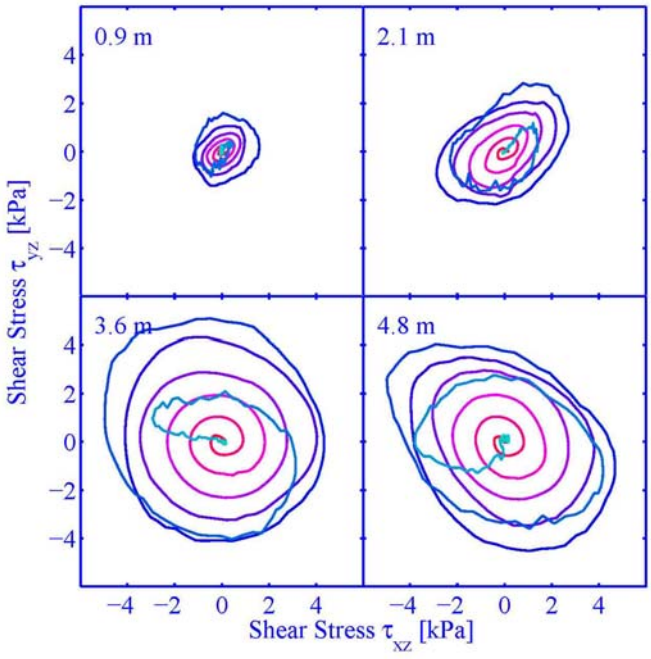

Fig. 5. Cyclic shear stresses on the xy plane at selected depth locations.

Microscale energy dissipation mechanism

During seismic loading, individual energy components were continuously monitored using the equations given in Table 1. The energy components presented herein are categorized as either input energies or dissipated energies. The energy that is being introduced to the system (input energy) is that due to the interaction of the base wall with the particles in the deposit (boundary energy, E_w), the body forces due to particles own weight (body energy, E_b), and the drag forces exerted by the pore-fluid (those include buoyancy and pressure gradient contributions–fluid drag energy, E_i). The dissipated energy is that resulting mainly from inter-particle sliding (friction energy, E_f), kinetic energy due to particle motion (E_k), normal and shear strain energies stored at particle contacts (E_{ns} and E_{ss}), and particle-to-particle impacts at the contacts (damping energy, E_d).

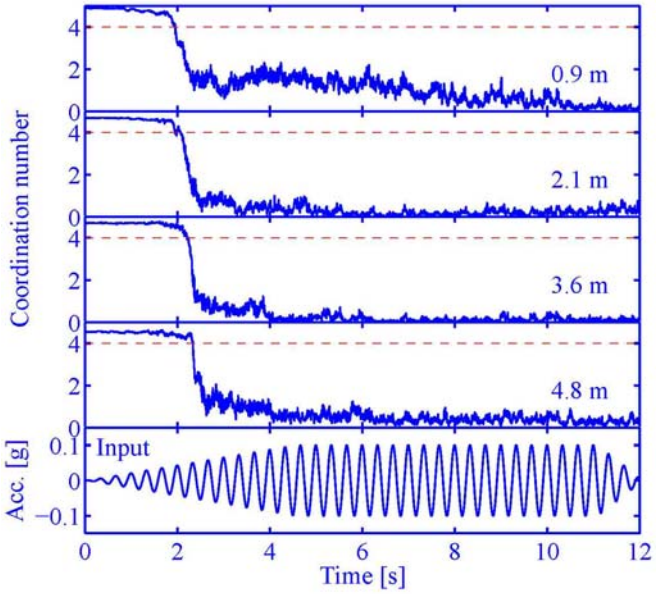

Fig. 6. Time histories of coordination number at selected depth locations.

Figure 7 shows the time histories of the cumulative input energy components (per unit volume of the deposit) for the first three seconds of the simulation. This time frame allows for an in-depth look at the behavior and magnitude of the individual energy components up to liquefaction. These energy components have been initialized such that they start from zero in the beginning of the loading phase. The figure indicates that boundary energy steadily increases up until liquefaction, after which it accumulates energy at a much decreased rate. This is due to the fact that the base wall is steadily introducing energy to the system as the input acceleration increases, and although the base acceleration continues to increase for the 3-second period, the majority of the particles are essentially floating after liquefaction takes place and the weight of the particles providing the normal force on the base wall significantly reduces. The body energy also steadily increases up to liquefaction, and at the onset of liquefaction shows a sharp increase in the rate of energy accumulation. This increase reflects the tendency of the particles to settle and densify after the onset of liquefaction. The fluid drag energy was decomposed into its three constituents in the *x*, *y*, and *z* directions. The fluid drag energy in the z-direction follows the same behavior as the body energy, but with the opposite sign, as drag energy is calculated from upward forces applied to the particles in motion. Fluid drag in the *x* and *y*-directions are negligible for this time period.

Figure 8 shows the time histories of the cumulative dissipation energy components for the same period up to liquefaction. The main source of energy dissipation prior to liquefaction is inter-particle sliding (friction), which increases with time up until liquefaction when its rate decreases due to the release of contacts. The elastic normal strain energy at the contacts also contributes to the total dissipated energy up to liquefaction, after which there is no additional energy dissipated through normal strain, again due to the fact that the particles are no longer in contact. Impact damping, kinetic, and contact shear strain energies do not play a significant role in energy dissipation for the first three seconds of the simulation.

Figure 9 illustrates the time histories of the input energy components for the entire duration of the simulation. The figure indicates that the body energy significantly contributes to the input energy from about 3 s into shaking until a time of about 40 s. This is, again, due to the increase in movement following liquefaction of the deposit, up until the particles have completely settled at 40 s. The boundary energy stopped accumulating post liquefaction, and drag energy in the *x* and *y* directions continued to be negligible for the 50 s time period. The fluid drag force in the z-direction initially decreases after liquefaction and then begins to increase until it also levels off after settlement ends.

Figure 10 shows that the main source of dissipated energy post liquefaction is friction, as the moving particles make periodic contacts after liquefaction. Impact damping energy begins to buildup at this time as well, as the particles gain velocity and continuously collide. This increase in particle velocity also explains the increase in the amplitude of the kinetic energy component between 3 s and 20 s.

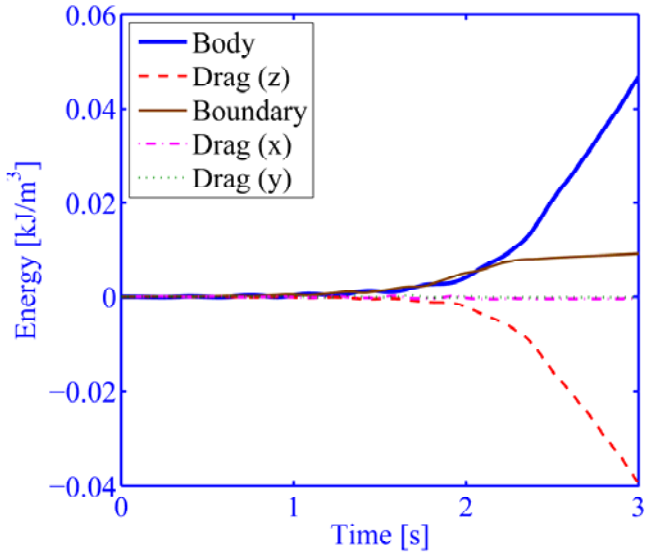

Fig. 7. Time histories of input energy components up to liquefaction.

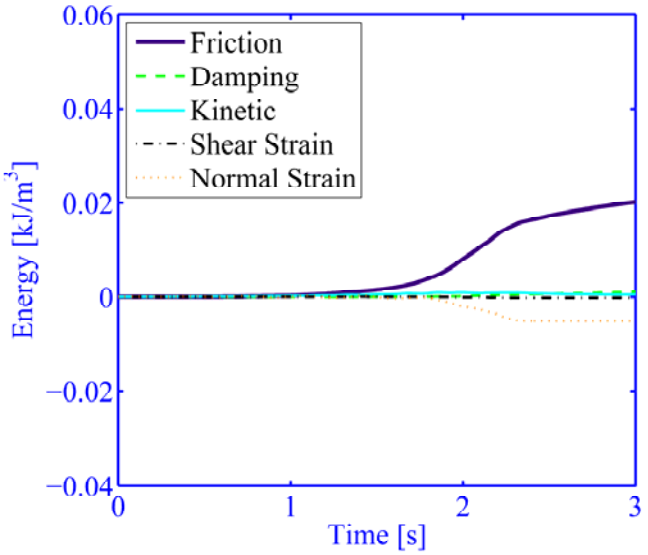

Fig. 8. Time histories of dissipated energy components up to liquefaction.

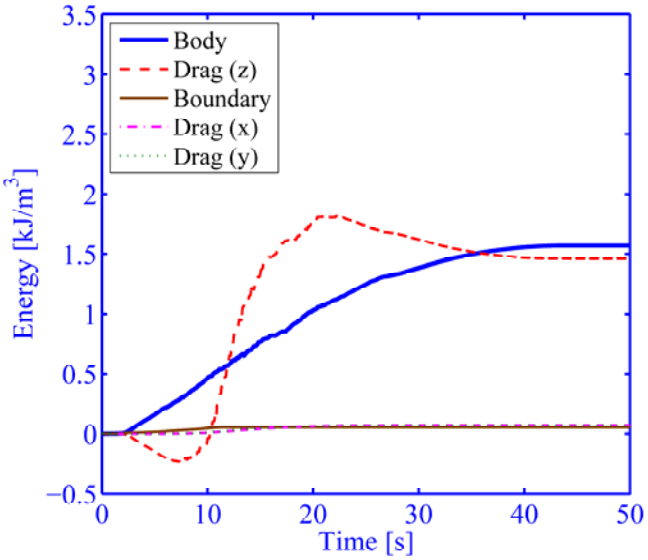

Fig. 9. Time histories of input energies for the duration of simulation.

Figure 11 shows the conservation of energy for the duration of the simulation (50 s). The amount of energy dissipated is almost equal to the amount of input energy for the entire simulation. Note that a small discrepancy starts to appear around the 12 s mark due to numerical integration errors resulting from the employed central finite difference time integration scheme in which velocities are assumed to be constant within a time step.

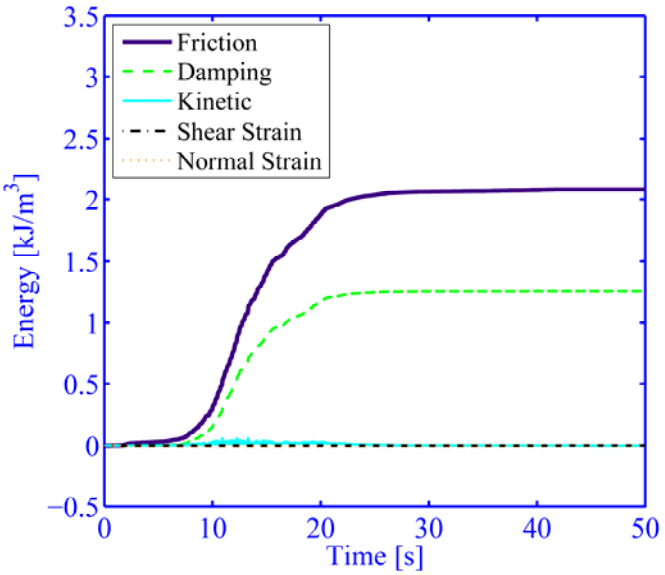

Fig. 10. Time histories of dissipated energies for the duration of simulation.

CONCLUSIONS

A microscopic energy monitoring technique is presented herein and applied to characterize energy dissipation mechanisms in saturated granular deposits subjected to seismic base excitations. An in-depth look at the microscale energy components leading up to liquefaction as well as after liquefaction took place revealed that prior to liquefaction energy is dissipated mainly through inter-particle sliding (friction energy), but after liquefaction particle-to-particle impact damping also plays a major role in dissipating energy. More results and interpretations are being published elsewhere.

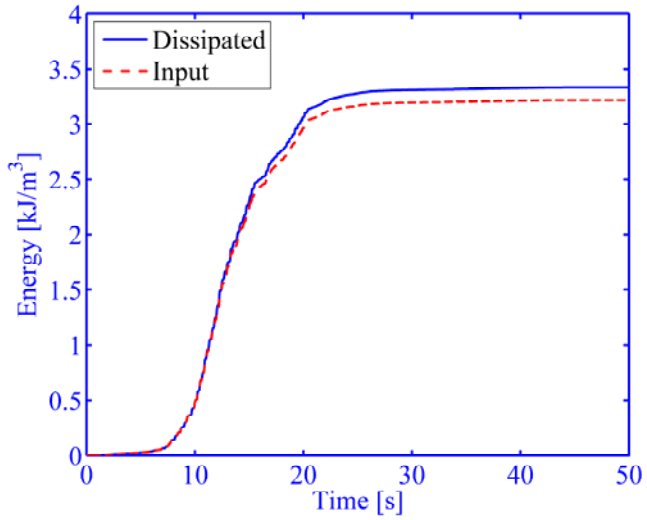

Fig. 11. Conservation of energy for duration of simulation.

REFERENCES

Asmar, B., Langston, P., Matchett, A., and Walters, J. [2003]. "Energy monitoring in distinct element models of particle systems." Advanced Powder Technology, 14(1), 43–69.

Bathurst, R. and Rothenburg, L. [1988]. "Micromechanical aspects of isotropic granular assemblies with linear contact interactions." Journal of Applied Mechanics, 55, 17–23.

Comiti, J. and Renaud, M. [1989]. "A new model for determining mean structure parameters of fixed beds from pressure drop measurements: application to beds packed with parallelepipedal particles." Chemical Engineering Science, 44, 1817–1823.

Cundall, P. and Strack, O. [1979]. "A discrete numerical model for granular assemblies." Geotechnique, 29(1), 47–65.

Davis, R. and Berrill, J. [1982]. "Energy dissipation and seismic liquefaction in sands." Earthquake Engineering and Structural Dynamics, 10, 59–68.

Dobry, R. and Ng, T. [1992]. "Discrete modeling of stress-strain behavior of granular media at small and large strains." Engineering Computations, 9, 129–143.

Edwards, S. [1998]. "The equations of stress in a granular material." Physica A, 249, 226–231.

El Shamy, U. [2004]. "A coupled continuum-discrete fluid-particle hydromechanical model for granular soil liquefaction," PhD Thesis, Rensselaer Polytechnic Institute.

El Shamy, U., and Denissen, C. [2009a]. "Microscale characterization of energy dissipation mechanisms in liquefiable granular soils." International Journal for Numerical and Analytical Methods in Geomechanics, Under review.

El Shamy, U. and Denissen, C. [2009b]. "A microscale energy approach for granular soil liquefaction." Journal of Engineering Mechanics, ASCE. Under review.

El Shamy, U. and Zeghal, M. [2005a]. "A coupled continuum-discrete model for saturated granular soils." Journal of Engineering Mechanics, ASCE, 131(4), 413–426.

El Shamy, U. and Zeghal, M. [2005b]. "A micro-mechanical study of the seismic response of saturated cemented deposits." Journal of Earthquake Engineering, 9, 47–75. Special Issue 1 on Geotechnical Earthquake Engineering.

El Shamy, U. and Zeghal, M. [2007]. "A micro-mechanical investigation of the dynamic response and liquefaction of saturated granular soils." Journal of Soil Dynamics and Earthquake Engineering, 27, 712–729.

Ergun, S. [1952]. “Fluid flow through packed columns.” Chemical Engineering Progress, 43(2), 89–94.

Evgin, E. [2000]. “An experimental study and numerical simulation of liquefaction at a soil-structure interface.” Proceedings, 53rd Canadian Geotechnical Conference: Geotechnical Engineering at the dawn of the 3rd Millennium, Canadian Geotechnical Society, Richmond, B.C., Canada. 1075–1082.

Figueroa, J. [1990]. “A method for evaluating soil liquefaction by energy principles.” Proceedings of 4th U.S. National Conference on Earthquake Engineering, Earthquake Engineering Research Institute, El Cerrito, California.

Figueroa, J., Saada, A., Liang, L., and Dahisaria, M. [1994]. “Evaluation of soil liquefaction by energy principles.” Journal of Geotechnical Engineering, ASCE, 120(9), 1554–1569.

Itasca [2005]. Particle Flow Code, PFC3D, release 3.1. Itasca Consulting Group, Inc., Minneapolis, Minnesota.

Jackson, R. [2000]. The dynamics of fluidized particles. New York: Cambridge University Press, Cambridge, U.K.

Law, K. and Cao, Y. [1990]. “An energy approach for assessing seismic liquefaction potential.” Canadian Geotechnical Journal, 27, 320–329.

Liang, L., Figueroa, J., and Saada, A. [1995]. “Liquefaction under random loading: unit energy approach.” Journal of Geotechnical Engineering, ASCE, 121(11), 776–781.

Nemat-Nasser, S. and Shokooh, A. [1979]. “A unified approach to densification and liquefaction of cohesionless sand in cyclic shearing.” Canadian Geotechnical Journal, National Research Council of Canada, 16, 659–678.

Ng, T. [1989]. “Numerical simulation of granular soil under monotonic and cyclic loading: a particulate mechanics approach,” PhD Thesis, Rensselaer Polytechnic Institute.

Rajamani, R., Mishra, B., Venugopal, R., and Datta, A. [2000]. “Discrete element analysis of tumbling mills.” Powder Technology, 109, 105–112.

Thevanayagam, S., Kanagalingam, T., and Shenthan, T. [2003]. “Intergrain friction, contact density, and cyclic resistance of sands.” Proc. of 2003 Pacific Conference on Earthquake Engineering, Christchurch, New Zealand.

Thornton, C. and Liu, L. [2000]. “DEM simulations of uni-axial compression and decompression.” Compaction of Soils, Granulates and Powders, D. Kolymbus and W. Fellin, eds., Balkema, Rotterdam, 251–261.

Yanadida, T., Matchett, A. J., and Coultard, J. [2001]. “Dissipation energy of powder beds subject to vibration.” Chemical Engineering Research and Design, 79, 655–662.

Zhang, D. and Whiten, W. [1998]. “An efficient calculation method for particle motion in discrete element simulations.” Powder Technology, 98(3), 223–230.